biosensors

MDPI

Article

Cultured Vagal Afferent Neurons as Sensors for Intestinal Effector Molecules

Gregory Girardi[1], Danielle Zumpano[2], Noah Goshi[1], Helen Raybould[2] and Erkin Seker[3,*]

Departments of [1]Biomedical Engineering, [2]Physiology and Cell Biology, and
[3]Electrical and Computer Engineering
University of California – Davis, Davis, CA 95616, USA
*Corresponding Author Information: 3177 Kemper Hall, Department of Electrical and Computer Engineering, University of California – Davis, Davis, CA 95616, USA; .
email: eseker@ucdavis.edu; Tel: +1 (530) 752-7300

Abstract: The gut-brain axis embodies the bidirectional communication between the gastrointestinal tract and the central nervous system (CNS), where vagal afferent neurons (VANs) serve as sensors for a variety of gut-derived signals. The gut is colonized by a large and diverse population of microorganisms that communicate via small (effector) molecules, which also act on the VAN terminals situated in the gut viscera and consequently influence many CNS processes. However, the convoluted in vivo environment makes it difficult to study the causative impact of the effector molecules on VAN activation or desensitization. Here, we report on a VAN culture and its proof-of-principle demonstration as a cell-based sensor to monitor the influence of gastrointestinal effector molecules on neuronal behavior. We initially compare the effect of surface coating (poly-L-lysine vs. Matrigel) and culture media composition (serum vs. growth factor supplement) on neurite growth, as a surrogate of VAN regeneration following tissue harvesting, where Matrigel coating but not the media composition played significant role in increased neurite growth. We then used both live-cell calcium imaging and extracellular electrophysiological recordings to show that the VANs respond to classical effector molecules of endogenous and exogenous origin (cholecystokinin serotonin, capsaicin) in a complex fashion. We expect this study to enable platforms for screening various effector molecules and their influence on VAN activity assessed by their information-rich electrophysiological fingerprints.

Keywords: Primary Neuron Culture; Electrophysiology; Microfluidics; Gut-Brain Axis

1. Introduction

The human gastrointestinal (GI) tract is colonized by a diverse population of bacteria that communicate with each other via small effector molecules. Effector molecules are not only gut-derived hormones but also are dietary and microbial metabolites. Growing evidence suggest that effector molecules regulate energy homeostasis, immune responses, as well as even overall behavior, in part by signaling to the central nervous system (CNS) [1–5]. Despite the large anatomical distance between the GI tract and brain, these two organs can communicate via the vagus nerve, a bi-directional communication pathway [6]. The vagus nerve is heavily involved in relaying satiety signals from the periphery to the brain, and motor signals for digestion from the brain to the periphery. Dysbiosis of the gut microbiome can be induced by a number of factors e.g., diet, food allergies, pharmaceuticals, can all disrupt the effector molecule profiles in the GI tract [7–9], which manifest itself as alterations of many physiological phenomena, including CNS function. An understanding of the role of these effector molecules in physiological states is currently in its infancy. It is difficult to draw causative conclusions between the gut microbiota and its influence on physiological phenomena, especially via the vagal route, because there are many

simultaneous confounding biological processes [10]. Therefore, *in vitro* models, such as cell culture are advantageous since they provide a reductionist approach to studying the influence of effector molecules on cells that range from intestinal epithelium [11,12] to neurons [13,14]. In addition, *in vitro* models, such as cell culture, can be readily probed by live-cell calcium imaging and intra-/extra-cellular electrophysiological recording [15,16].

The vagus nerve is the main link between the brain and GI tract. The vagus nerve is composed of afferent and efferent fibers, transmitting signals from the periphery to the CNS or from the CNS to the periphery, respectively [17]. Here, we focus on the afferent signals that are initiated in the periphery (gut) and are then transmitted back to the CNS via afferent neurons. *In vivo*, the neuronal cell bodies responsible for afferent transmission reside in the nodose ganglion, which is located lateral to the carotid artery. Vagal afferent neurons (VANs), richly innervate the intestinal mucosa and express receptors for many known bacterial metabolites, as well as mechanical receptors for sensing tissue stretch [18–20]. Others have shown that VANs respond to several effector molecules such as gut hormones and paracrine mediators. For example, cholecystokinin (CCK), a peptide hormone produced from the gastrointestinal tract in response to the digestion of fat and protein, depolarizes VANs both *in vivo and in vitro* [21,22]. Serotonin (5-HT), an important neurotransmitter also depolarizes VANs [23]. Finally, capsaicin (Cap), an active component in chili peppers, results in depolarization of VANs [24]. This short list is a mere fraction of gastrointestinal effector molecules with various origins (e.g., CCK [endogenous], 5-HT [endogenous, bacteria-produced], Cap [ingested plant alkaloid]), that have the potential to signal to VANs. [6,25]. Considering that recent work has shown that microbiota-derived molecules can modulate electrophysiological activity of VANs, they are promising candidates to serve as "living" biochemical sensors for screening effector molecules. To that end, intracellular calcium imaging and patch-clamp-based intracellular electrophysiological recordings have been the main techniques for studying the influence of effector molecules [15,24,26]. While these approaches produced important insight into how effector molecules modulate VAN activity, they have some shortcomings. For example, calcium imaging reveals time-varying concentrations of intracellular calcium due to external stimuli; however, some of these fluxes may only create subthreshold membrane potentials, hence not resulting in full action potentials that drive the signal propagation from the gut to the CNS. On the other hand, while patch-clamp provides accurate measurements of membrane potential fluctuations, it is a labor-intensive technique that requires significant expertise and its neuron-by-neuron interrogation nature is inherently low throughput. Extracellular recordings circumvent some of the challenges associated with the two techniques by exclusively capturing extracellular spikes (local field potentials) and being amenable to scale-up by increasing the number of electrode sites (thousands of channels) while maintaining single cell resolution through post-processing of electrophysiological signals. Surprisingly, VANs have not been integrated with extracellular recording-based approaches to monitor the influence of effector molecules on their activity, in part due to their low cell yield compared to cortical cells for example, which impose challenge on extracellular recordings. In this study, we report on establishing a primary rat VAN culture in combination with common electrophysiological readouts (calcium imaging and extracellular recordings) and demonstrate their potential to screen physiological effector molecules. This work shows that this novel *in vitro* tool has the potential to bridge the gap between *in vivo* and *in vitro* studies to isolate the effects of microbial metabolites on VAN activity in a physiologically relevant format and advance the understanding of the gut-brain axis.

2. Materials and methods

2.1. Cell culture surface preparation

Cell morphology characterization to probe neuronal health were conducted on glass slides (Premium Cover Glass, Fisher Scientific, 12548B) coated with either poly-L-lysine

(PLL, Sigma, P1399, 0.5 mg/ml) in B-buffer (3.1 mg/ml boric acid and 4.75 mg/ml borax) or poly-D-lysine (PDL, Gibco, A38904-01, 0.1 mg/ml) and Matrigel (Corning, 354230, 0.2 mg/ml, H_2O). All glass slides, irrelevant of their coating material were sprayed with 70% ethanol, dried with N_2 air, then plasma cleaned for 1 min at 10 W (repeated for both sides). PLL slides were then incubated with PLL for 4 hours, washed 6 times with sterile DI water, and then flooded with media overnight prior to cell seeding the following day. PDL/Matrigel slides were plasma cleaned for 1 min at 10 W (repeated both sides) and incubated with PDL for 15 mins, washed 5 times with sterile DI water, incubated with Matrigel for 30 mins, then rinsed and stored in incubator with sterile DPBS containing calcium and magnesium (DPBS+, Gibco, 14040133) until cell seeding. PDL/Matrigel slides were prepared the morning of cell harvesting, while PLL slides were prepared the day prior. Calcium imaging experiments to probe electrophysiological response were conducted on glass slides treated with PDL/Matrigel following steps outlined above. Microelectrode array (MEA) experiments for extracellular recordings utilized both in-house fabricated platforms which were coated with PDL/Matrigel following the steps outlined above, as well as commercial high-density MEA (HD-MEA, Maxwell Biosystems, Zurich, Switzerland) also coated with PDL/Matrigel without plasma treatment.

2.2. Vagal afferent neuron dissection and culture

Male Wistar rats (5 weeks old) purchased from Envigo were used to obtain vagal afferent neurons. All tissue harvesting procedures were approved by the Institutional Animal Care and Use Committee at University of California, Davis. Animals were housed under 12 h light/12 h dark conditions and fed standard pellet chow ad libitum. Vagal afferent neurons were harvested following previously established protocols [26]. Briefly, nodose ganglia were isolated bilaterally from rats under anesthesia via isoflurane (VetEquip V-1 Tabletop with Active Scavenging). Following a midline incision in the neck, the musculature was retracted, and blunt dissection techniques were used to separate the vagal nerve from the carotid artery. Under magnification (AmScope LED-144A), remove the nodose ganglia and place in Hank's balanced salt solution, calcium, magnesium (HBSS+ 1X, Thermo Fisher, 14025092) while isolating the second nodose. Once harvested, nodose ganglia were desheathed and digested in HBSS [-] (Gibco, 14185-052, H_2O, 1x) containing 1 mg/ml of both collagenase type 1A (Worthington, LS004188) and dispase II (Roche, 04942078001) for 90 min at 37ºC in 95% air/5% CO_2. Neurons were dispersed via gentle trituration and then washed in growth factor-based medium (described next). Dispersed cells were plated (density varied for application, see relevant sections below) on desired surface and relevant medium (37ºC in 95% air/5% CO_2).

Serum-based media is comprised of Dulbecco's Modified Eagle Medium (DMEM, Sigma-Aldrich, D5030-102, H_2O, 8.3 g/L), fetal bovine serum (FBS, HyClone, SH30071.03, 10% v/v), GlutaMAX (Thermo Fisher, 35050061, 0.5 mM), HEPES (Thermo Fisher, 15630080, 10 mM), glucose (Thermo Fisher, A2494001, 5 mM), sodium pyruvate (Thermo Fisher, 11360070, 0.227 mM), and sodium bicarbonate (Thermo Fisher, 25080094, 2.2 g/L). *Growth factor-based media* is comprised of Dulbecco's Modified Eagle Medium (DMEM, Thermo Fisher, 11885084, 46% v/v), Bovine Serum Albumin, (BSA, Sigma-Aldrich, A8806, DMEM, 0.5 mg/ml), GlutaMAX (Thermo Fisher, 35050061, 1.4 mM), Selenium/Insulin/Trasnferrin (ITS-G, Thermo Fisher, 41400045, 30 nM), Nerve Growth Factor (2.5S NGF, Envigo, B.5017, 125 ng/ml), and Ham's F-12 Nutrient Mix (Thermo Fisher, 11765054, 49% v/v) [27]. Medium contents are presented with the following format when appropriate: Name (Abbreviation, vendor, catalog number, solvent, working concentration).

2.3. Effector molecules

Effector molecules that depolarize VANs were used [23,24,26]: Cholecystokinin octapeptide, sulfated (CCK, Tocris, 1166, DPBS+, 10 nM) [26]; serotonin hydrochloride (5-HT, Sigma-Aldrich, H9523, H_2O, 100 μM) [23]; capsaicin (Cap, Tocris, 0462, ethanol, 1 μM)

[13,24]. Elevated extracellular potassium chloride (KCl, 20 mM) with an equimolar reduction of NaCl was used as a positive control [28]. Ethanol (same working concentration with Cap) was used as the vehicle since other diluents (e.g., DPBS+) do not generally affect cell viability and function. Effector molecules are presented with the following format: Name (Abbreviation, vendor, catalog number, solvent, working concentration).

2.4. Intracellular calcium flux measurements

The harvested neural cells from each rat (two nodose ganglion) were split across three glass slides for the calcium imaging studies. At the final centrifugation of the cell dissociation, the pellet was resuspended at a final volume of 150 µl in culture media, of which 50 µl fractions were used for plating the cells on each slide. The slides were then placed in the incubator for 1.5 hr to allow for cell attachment, after which, 3 mL of media was gently flooded over each slide. All calcium imaging was performed at room temperature (22°C) and 24 hours after cell seeding. Calcium transients were monitored by use of the fluorescent calcium indicator Fluo-4 AM (Thermo Fisher F14201). Cells were prewashed with HBSS+, followed by incubation with 3 µM Fluo-4 AM for 60 mins at room temperature (22ºC) in HBSS+, followed by another subsequent wash in HBSS+, per the protocol from the vendor. After the final wash, slides with the cells were placed into a new 6 well plate and placed on the microscope (Zeiss Axio Observer D1). Images (Excitation 488 nm, Emission 520 nm) were collected every 6 secs over the imaging duration. The neuronal cell bodies were identified by their large size (~50 µm diameter) and spherical shape, and marked as a region of interest (ROI) within ImageJ [29]. The time-varying change in fluorescence intensity within the ROIs were then quantified from the time-lapse images acquired during calcium imaging. The intensity was normalized to each corresponding cell's baseline intensity value, providing a relative *fold change* quantity that was plotted against the imaging time course.

2.5. Immunocytochemistry and imaging

The slides with the cells were washed 3 times with 37°C DPBS+ and fixed with 4% w/v paraformaldehyde (PFA, Affymetrix) in DPBS+ for 1 hour at room temperature. After fixation the cells were washed 3 times with DPBS+, twice with 0.05% v/v Tween20 (Sigma, DPBS+), followed by a 3-minute permeabilization with 0.1% v/v Triton X-100 (Thermo Fisher, DPBS+) and two additional washes with the Tween20 solution. The coverslips were then blocked with 0.5% v/v heat-inactivated goat serum (Thermo Fisher) and 0.3 M glycine (Sigma) in DPBS+ (blocking buffer) for 1 hour. Following the blocking step, samples were incubated for 1 hour with primary antibody solution containing mouse anti-βIII tubulin (βT-III; Thermo Fisher, 1:500) and rabbit anti-NeuN (Thermo Fisher, 1:500) in blocking buffer (without glycine). For cultures stained for supporting cells, primary antibody solution contained mouse anti-βIII tubulin (βT-III; Thermo Fisher, 1:500) and rabbit anti-GFAP (Thermo Fisher, 1:100) in blocking buffer (without glycine). Samples were then washed 3 times with Tween20 solution, then followed by a 1-hour incubation with secondary antibody solution containing goat anti-mouse conjugated to AlexaFluor 555 (Thermo Fisher, 1:500) and goat anti-rabbit conjugated to AlexaFluor 488 (Thermo Fisher, 1:500) in DPBS+. For cultures stained for supporting cells, secondary antibody solution contained goat anti-mouse conjugated to AlexaFluor 647 (Thermo Fisher, 1:500) and goat anti-rabbit conjugated to AlexaFluor 488 (Thermo Fisher, 1:500) in DPBS+. Following incubation with the secondary antibody solution, the samples were washed 3 times with DPBS+, then incubated for 5 minutes with a 4',6-diamidino-2-phenylindole (DAPI) solution (Sigma, 1:20000, H_20). Samples were then washed with Tween20 a final time prior to mounting slides onto a glass slide (Globe Scientific, 1324B) using ProLong Gold Antifade Mountant (Thermo Fisher). The cells were imaged at three random locations on each slide. The images were then analyzed using a custom ImageJ script to quantify area coverage of

βT-III stain. The βT-III area coverage was then normalized to the number of neurons in each image (quantified by counting the NeuN-stained cell bodies).

2.6. In-house Fabricated Micro Electrode Arrays

Custom MEAs were fabricated using previously described methods [16]. Briefly, MEAs were designed using a 4 x 8 array of electrodes (32 total) each with a diameter of 20 μm and interelectrode pitch of 130 μm. The electrodes and traces (250 nm-thick Au over a 160 nm-thick Cr adhesion layer) were sputter-deposited on borosilicate glass wafers (500 μm thick, University Wafers) and patterned using standard lift-off techniques. SiO_2 (200 nm) was deposited via plasma-enhanced chemical vapor deposition to serve as the insulation layer. Finally, the electrode sites were lithographically masked with patterned photoresist and opened via a brief immersion in buffered oxide etch. Individual MEAs were separated with a dicing saw (Disco DAD 321). Glass cloning cylinders (8 mm × 6 mm inner diameter, Sigma, MI, USA) were attached over the MEA using sterile vacuum grease (Dow Corning, Midland, MI, USA) to serve as cell culture chambers. A schematic of the fabrication process is shown in **Figure S1**.

The harvested neural cells from each rat (two nodose ganglion) were seeded onto a single MEA to attain high cell density. The MEA was then placed into a custom-built rig and placed into the incubator at 37ºC in 95% air/5% CO_2 for the duration of the recording. Recordings were performed at a sampling frequency of 30 kHz using an RHD2132 Intan amplifier (Intan Technologies, Los Angeles, CA, USA). The neuronal activity was recorded for 5 mins initially to capture baseline extracellular electrophysiological activity, followed by sequential additions of vehicle, CCK (10 nM), Cap (1 μM), and KCl (20 mM). A 30-second equilibration period following addition of effector molecules was used prior to initiating the recording to minimize recording noise artifacts both from perturbation of the liquid over the electrodes and mechanical noise from accessing the incubator. The acquired electrophysiological signal was processed in Offline Sorter (Plexon, Dallas, TX, USA), where the signal was high pass filtered (300 Hz cut-off) and any features with an amplitude 8 times above or below (dual thresholding) the standard deviation of the noise were extracted as spikes. Since dual thresholding, 5 ms of signal after every spike detection was thrown out to avoid double counting spikes. Spikes were sorted in Offline Sorter using the valley-seeking algorithm, with a Parzen multiplier of 2.0.

2.7. High-Density Micro Electrode Arrays

A commercial CMOS-based high-density microelectrode array (HD-MEA, Maxwell Biosystems, Zurich, Switzerland) was subsequently used to allow recordings from a large number of cells [30]. The HD-MEA consists of 26,400 platinum black microelectrodes distributed within a recording area of 3.85 x 2.10 mm^2 (3,265 microelectrodes per mm^2). The microelectrodes can be activated in arbitrary patterns to allow for recordings from 1,024 individual channels at a time.

For electrophysiological measurements, the HD-MEAs were placed into the MaxOne Single-well MEA recording rig and maintained at 37ºC in 95% air/5% CO_2 during the recordings. Similar to the recording protocol with the custom MEA described earlier, an initial 5-min recording was conducted to capture baseline electrophysiological activity, followed by sequential additions of vehicle solution and various effector molecules: CCK (10 nM), 5-HT (100 μM), Cap (1 μM), followed by a positive control of elevated extracellular KCl (20 mM). Again, implementing a 30-second equilibrium period prior to initiating the recording to reduce noise artifacts as mentioned above. A 5-min recording was performed for each condition. The signal acquired at 20 kHz was band-pass filtered (300 – 7000 Hz) and the features with an amplitude 5.5 times above the standard deviation of the noise were counted as spikes. In addition, any time-series signal with less than 30 spikes

over the 5-minute recording window (6 spikes/min or 0.10 Hz) were excluded from further analyses.

2.8. Statistical Analysis

To compare the role of surface coating and culture media composition on neuronal coverage, a two-way ANOVA was performed with Šídák's multiple comparison test. A similar statistical analysis was used to compare non-neuronal cell count for the different surface coatings and culture media composition. A one-way ANOVA with Dunnett's multiple comparison test was used to compare the fluorescence intensity change in Fluo-4-loaded VANs in response to the effector molecule additions. For cell morphology studies, a total of 4 biological replicates, each producing 3 technical replicates was used. Each technical replicate was imaged at three random locations. For calcium imaging studies, a total of 8 biological replicates, each producing 3 technical replicates were used. The custom MEA data is from the cell culture established from a single biological replicate, while the HD-MEA data is from 3 biological replicates, where cells from each rat was plated into a separate HD-MEA to attain sufficient cell density over the electrode sites. For all statistical comparisons, a p-value < 0.05 was considered significant. All statistical analyses were performed in GraphPad Prism.

3. Results and Discussion

3.1. Influence of culture conditions on VAN morphology

Previous studies of VANs involving patch-clamp or calcium-imaging interrogation were primarily performed in acute settings (less than 24 hours in vitro [15,22,24,26,31,32]). Extracellular recordings, on the other hand, require longer culture durations for the cells to attach on or near the electrodes. This necessitates the optimization of culture conditions to quickly attain and sustain neuronal viability/function, one of which is neurite outgrowth. Dissociated VANs were cultured on glass coverslips coated either with PLL or Matrigel. PLL is commonly used in cell culture to promote neuronal cell attachment [33] and Matrigel, which consists of various cellular basement proteins, enhances in vitro neuronal network formation of rat cortical cells [34,35]. In addition, to surface coatings, two media types were also compared. A common media composition used for acute cultures of VANs is DMEM supplemented with 10% FBS (referred to as *serum-based media*) [15,22,24,26]. We hypothesized that a more specialized neuronal culture medium would better sustain neuronal cell viability and function in the non-acute cultures. Therefore, we also used a culture medium composed of 1:1 DMEM/F12 supplemented with NGF (referred to as *growth factor-based media*) [27]. Representative brightfield images of the cultures on day *in vitro* (DIV) 1 and 3 can be in seen in **Figure S2/S3**, where fixed immunostained images from DIV 3 can be seen in **Figure 1A**. Using the βT-III stain (shown in red), neuron coverage was quantified and then normalized to number of neurons, NeuN stain (shown in white) per field of view. Matrigel lead to a significant increase in percent neuronal coverage regardless of the media type (Two-way ANOVA: Media: $p = 0.1907$, Slide coating: $p < 0.0001$, Interaction: $p = 0.4781$. Šídák's multiple comparison: FBS: $p = 0.0174$, NGF: $p = 0.0033$), as shown in **Figure 1B**. In addition to neurons, dissociated cultures from the nodose have also been shown to include satellite cells, fibroblasts, and Schwann cells [36,37]. We distinguish these cells from the VANs by selecting DAPI-labeled regions that are not co-localized with NeuN (neuron soma specific). The number of non-neuronal cells as shown in **Figure 1C** was independent of the media type or surface coating. To confirm the presence of non-neuronal cells in the culture, we maintained the cultures for 7 days and immunostained them to confirm presence of supporting cells (**Figure S4**).

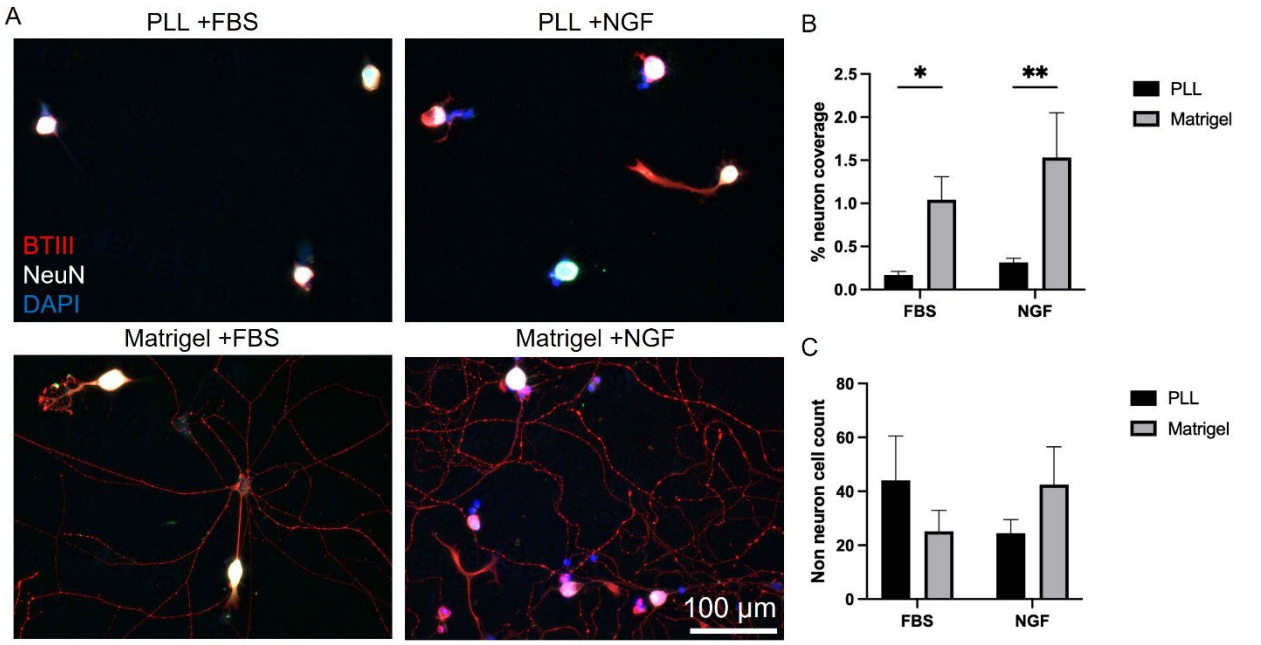

Figure 1. Vagal afferent neuron culture conditions. (A) Representative cell culture images for the different surface coating and media conditions. (B) Media comparison of serum-based media (FBS) to growth factor-based (NGF) on its role on percent neuron coverage. (C) Influence of surface coating and culture media type on non-neuron cell counts. * $p \leq 0.05$, ** $p \leq 0.01$. Error bars indicate standard error of the mean (SEM).

3.2. Live-cell calcium imaging

Live-cell calcium imaging has been used with VANs in acute cultures to quantify their response to various effector molecules [15,22,24,26]. We used a similar technique to confirm that the VAN cultures here are functional. In a single field of view with three VANs (distinguished by the cell soma fluorescing with Fluo-4; green), each neuron exhibits a different response. Specifically, the VAN within the red box only responds to Cap, whereas the VAN within the blue box responds to both 5-HT and Cap (**Figure 2A**). 5-HT and Cap both have depolarizing effects on the VANs [23,24], observed as increasing fluorescence intensity in response to their addition to the cultures (**Figure 2B**). The observation of two different VAN responses highlights the presence of subpopulations of VANs, as also reported by others [24]. **Figure 2C** summarizes the percent change of VANs' fluorescence intensity (surrogate for calcium activity) between pairs of conditions (i.e., baseline to vehicle, vehicle to 5-HT, and vehicle to Cap). 57 VANs across 8 biological replicates were quantified for their change in intracellular calcium in response to effector molecules, where a VAN had to exhibit 10% increase over the baseline fluorescence when exposed to Cap or KCl as an inclusion criteria. Such inclusion of a positive control (e.g., Cap or KCl) has also been used by others to exclude dead cells from analysis [24]. Interestingly, vehicle addition leads to a small increase in peak fluorescence over the baseline. We attribute this to the presence of mechanosensitive receptors on VANs, as also reported elsewhere [38]. For the subsequent analyses, we compare the cellular response of effector molecules to that of the vehicle's response. The VANs also respond to 5-HT (4 out 6 neurons) and Cap (51 out of 51 neurons) in comparison to the vehicle condition, with Cap resulting in a response much larger than the VAN's response due to transition to vehicle from baseline (One-way ANOVA, Dunnett's multiple comparison: $p = 0.0042$). Taken together, this shows that the VANs cultured on Matrigel with the growth factor-based media are capable of sensing and responding to classical effector molecules (5-HT and Cap) *in vitro*.

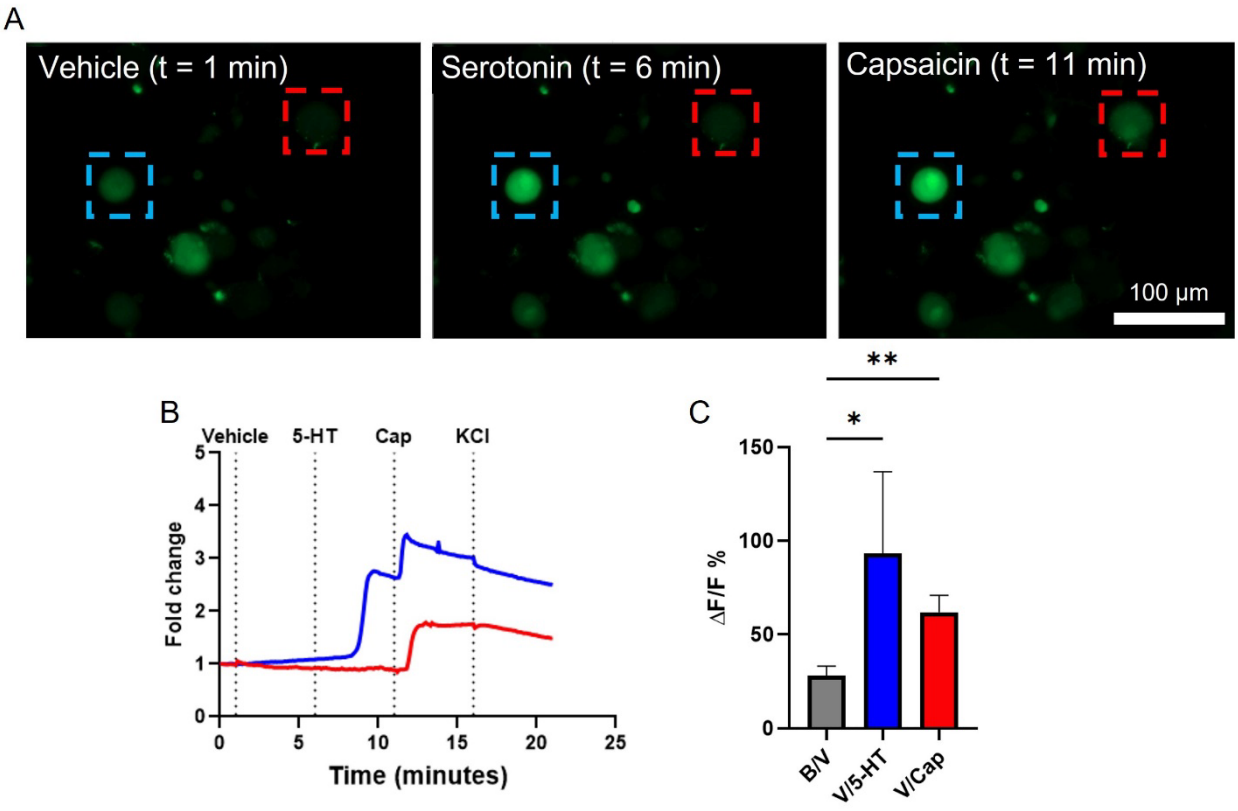

Figure 2. **Intracellular calcium activity in response to effector molecules.** VANs were incubated with Fluo-4 AM and their fluorescence intensity was tracked over time when exposed to 5-HT (100 µM) or Cap (1 µM). (A) A single field of view tracking several VANs over time as they were sequentially exposed to 5-HT then Cap. Blue box monitors a VAN that responds to both 5-HT and Cap, while the red box monitors a VAN that responds only to capsaicin. (B) Representative fold-change traces of intracellular calcium corresponding to the blue and red boxed cells shown in A. (C) Neurons pooled across 8 rats quantifying ΔF/F % for vehicle compared to baseline (57 neurons), and for 5-HT (6 neurons) or Cap (51 neurons) compared to vehicle respectively. * $p \leq 0.05$, ** $p \leq 0.01$. Error bars indicate standard error of the mean (SEM).

3.3. Extracellular Recordings of VANs

While intracellular calcium measurements are useful for providing insight into the responsiveness of the VANs to the effector molecules, extracellular electrophysiological recordings are often necessary to monitor manifestation of intracellular calcium fluxes as action potentials [39,40]. In addition, microelectrode arrays (MEA) allow for simultaneously monitoring neuronal activity in an area often larger than the field of view used for calcium imaging [41]. In this study, we used both in-house fabricated MEAs (**Figure 3A**), as well as a commercially available HD-MEA from Maxwell Biosystems. Cells from the dissociated nodose ganglion were cultured on the custom MEAs (**Figure 3A**), which consisted of 32 electrode sites with recording surface of (400 µm^2). Cells (including both VANs and non-neuronal cells) from one rat (two nodose ganglia) were seeded onto a single MEA (50 mm^2 seeding area) and cultured until DIV1 when recordings were conducted. A 5-min baseline recording, followed by CCK, Cap, and finally KCl addition was performed. To minimize neuronal detachment, the cells were not washed in between adding various effector molecules. Changes in spiking activity were evident in recordings following CCK and KCl addition (**Figure 3B**), which consisted of waveforms indicative of action potentials originating from the VANs (**Figure 3B** inset) by specific electrode sites (indicated with white arrows) in **Figure 3A**. The sorted spikes reveal one waveform following CCK addition and two distinct waveforms following KCl addition (yellow and green). The presence of two distinct waveforms suggests that two distinct neurons are contributing to the

signal, which is confirmed with the bright field image showing two neurons near the recording electrode (**Figure 3A** inset, white arrows highlighting each neuron). Collectively, this also demonstrates the presence of subpopulation of VANs that are responsive to different effector molecules.

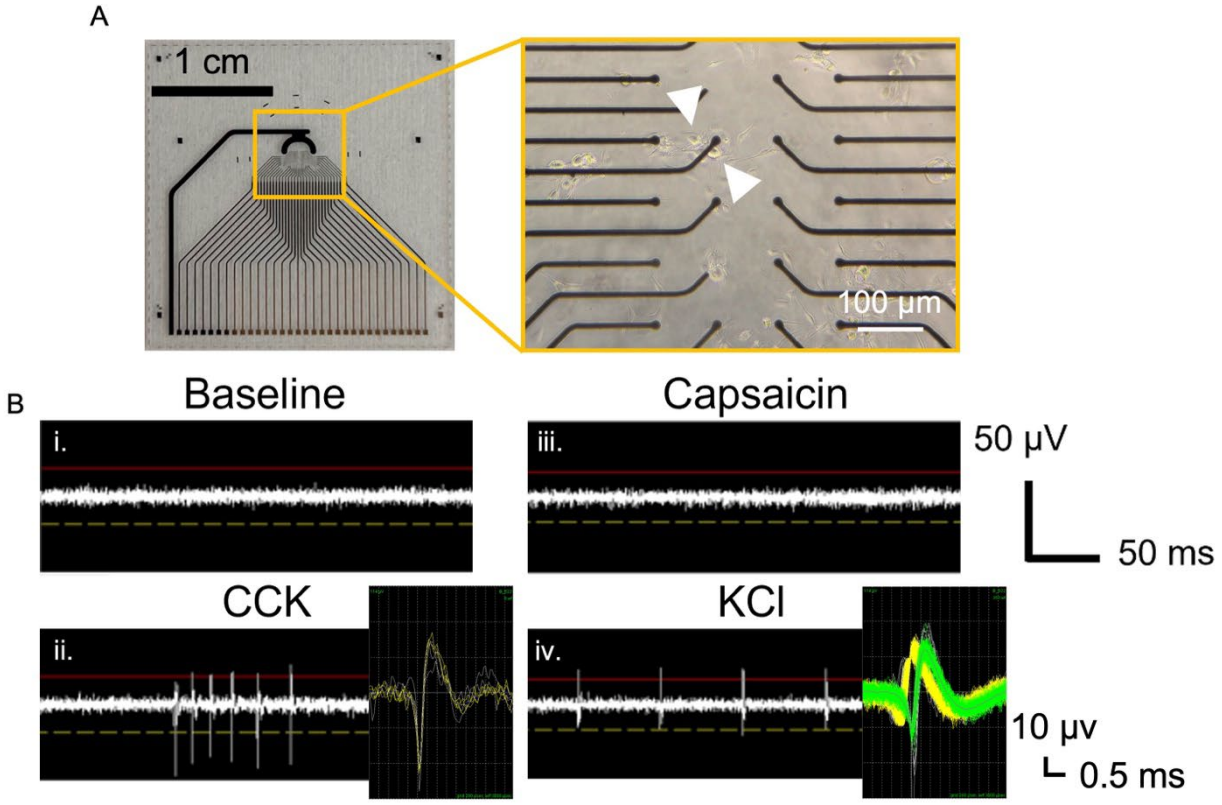

Figure 3. **Extracellular recordings from in-house fabricated MEAs.** (A) 32-electrode planar gold MEAs with bright-field image showing VANs adhered near the electrodes. (B) Extracellular recordings following sequential addition of CCK (10 nM), Cap (1 µM) and KCl (55 mM) from highlighted electrode in A. Arrows indicate the two VANs contributing to the recorded signal. Insets show spike-sorted waveforms, where the "KCl inset" reveals two distinct waveform shapes (shown by yellow and green waveforms), confirming recordings from two different neurons.

It is evident from micrographs of VANs cultured on surfaces (**Figures 1-3**) that the cell density is low. An adult rat has only ~12,000 VANs (6,000 per nodose) [36] and the net number of VANs available for seeding is inadvertently reduced due to the yield of the harvesting/dissociation process. Therefore, to attain a high seeding density, dissociated cells from one rat were plated on a single MEA. This is critical since to acquire extracellular activity from a neuron with sufficient signal-to-noise ratio, the electrode needs to be within 50 µm (one cell diameter in the case of the VANs) [42]. While this criteria is easily met for cultures with cortical and hippocampal cells, where a rat yields millions of neurons [13,16], the lower cell density of VANs poses a challenge for extracellular recordings. To address the issue of electrode-neuron distance and to improve the probability of having a VAN near an electrode, we transitioned to using a HD-MEA system from Maxwell Biosystems.

HD-MEAs employ CMOS technology to increase electrode site density. Similar to the protocol used for the custom MEAs, dissociated cells from one rat (two nodose ganglia) were seeded onto 1 HD-MEA (3.85 x 2.10 mm^2), using three rats for a total of 3 HD-MEA chips. For each HD-MEA, we configured the recording electrode topology to distribute the 988 electrodes evenly across the MEA culture surface. Each MEA was taken through the exact same recording sequence of baseline, vehicle, CCK, 5-HT, Cap, and KCl with 5-

min recordings for each condition. **Figure 4A** shows a 10-sec recording window from an individual neuron after exposure to each effector molecule. Qualitatively, differences in spiking activity are readily noticeable for the different conditions and the firing rate varies as a function of the added effector molecule (e.g., CCK and 5-HT, both depolarizing molecules [23,26]). Upon the addition of Cap, the spiking activity is subdued, which is surprising since Cap generally acts as a depolarizing molecule as shown by others [24] and also here in calcium imaging studies (**Figure 1**). The inhibition of spiking activity may be attributed to possible desensitization of VANs by potent Cap [43], which is discussed further later. A lack of spikes was also observed following KCl addition, which further supports residual desensitization from Cap exposure.

To provide a more holistic picture of the electrophysiological activity of VANs cultured on the 3 HD-MEAs, we created a composite raster plot (**Figure 4B**). In composing the raster plot, for an electrode (electrode = 1 neuron due to size of electrode) to be considered active, it needed to have at least a firing rate of 6 spikes/min, a spike frequency cutoff recommended by MaxWell to rule out any electrical noise that may appear as an actional potential. To further ensure that the spiking is due to the cultured VANs, we used a blank MEA (no cells) and performed the same recording protocol of sequentially adding the effector molecules. The resulting raster plot (created with the same signal processing criteria), shown in **Figure S5**, reveals negligible spike traces in comparison to HD-MEAs with cells (**Figure 4**). From the raster plot in **Figure 4B**, it is possible to monitor the time-sequence of neuronal activation and inhibition. There are various groups (subpopulations) of neurons that exhibit distinct activation/inhibition patterns in response to effector molecule exposure (**Figure 4C**). From the 15 neurons recorded, 2 neurons (12.50%) become active with CCK, 6 neurons (37.50%) turn off with Cap, 4 neurons (18.75%) turn on with 5-HT, 4 neurons (25%) turn off with 5-HT, and 1 neuron (6.25%) turn off with KCl. One of the neurons (neuron 6 in **Figure 4C**) can be binned in both the on at CCK and off at Cap group, so percentages reported are out of 16 total. These distinct activation/inhibition characteristics further supports the diversity of VANs and their functional subpopulations.

An interesting subpopulation of the VANs are the ones that turn off with Cap. Cap works through binding to the transient receptor potential cation channel subfamily V member I (TRPV1), a nonselective cationic channel [43]. Upon binding to its receptor, the influx of Na^+ and Ca^{2+} should lead to depolarization of the neuron [24]. However, as shown in **Figure 4C**, we observe 37.5% (6 neurons) become inactive when exposed to Cap. We hypothesize that the neurons could be strongly responding initially to the Cap prior to entering an inactive state, which is likely missed due to the intentional delayed start of recording. Specifically, upon addition of effector molecules and prior to starting the recording, we allow for a 30-second equilibration period to minimize recording noise artifacts both from perturbation of the liquid environment of the MEA and mechanical noise from accessing the incubator. It is possible that for neurons with TRPV1 receptors, the high working concentration (1 μM) results in a large depolarization, after which the neurons appear inactive on the raster plot. In addition, this subpopulation of VANs remains silent even after addition of KCl further supporting the Cap-induced desensitization. This was confirmed with the use of our intracellular calcium monitoring technique, where after identifying neurons that responded to Cap, we challenged them with KCl and observed no further increase in their intracellular levels of calcium (**Figure S6**).

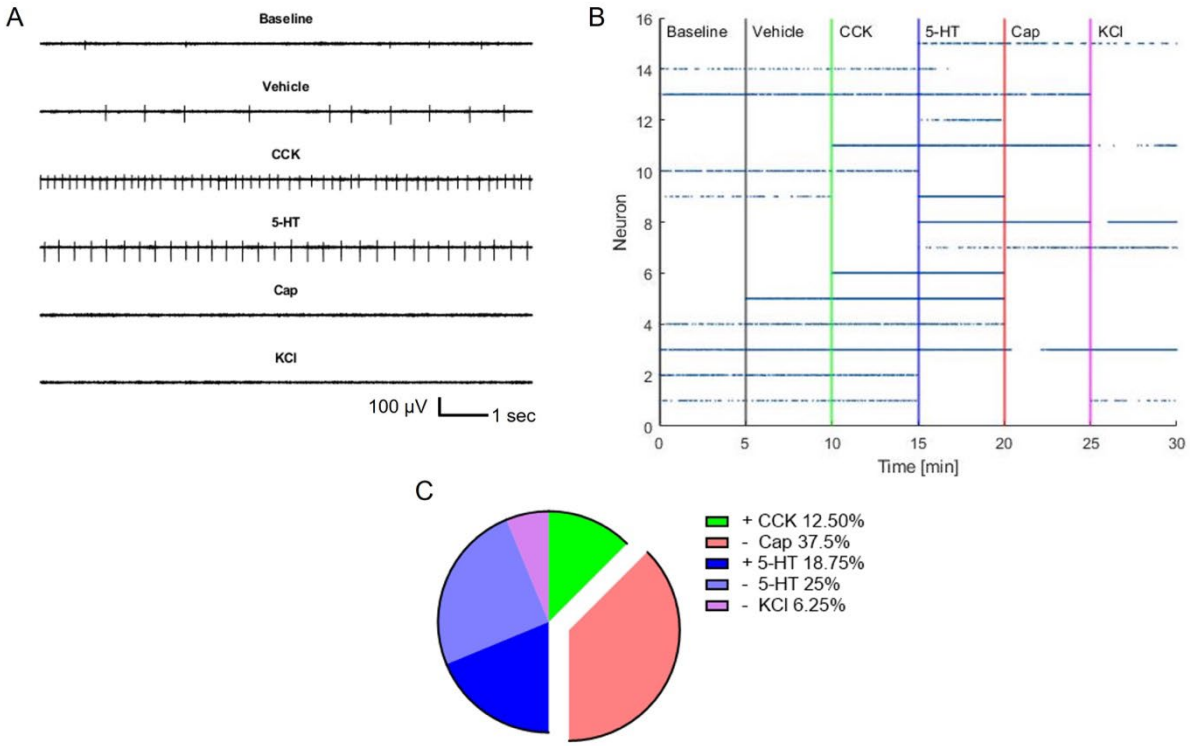

Figure 4. **Extracellular recordings from HD-MEA.** (A) The first 10 seconds of recording for each effector molecule from neuron 5 in panel B. (B) Raster plot highlighting active neurons pooled from 3 rats (15 neurons) across the effector molecule groups. (C) Summary of VAN activation/inhibition characteristics. .

MEA-based recordings allow for the extraction of wide range of electrophysiological parameters [42], including spike waveforms as illustrated earlier (**Figure 3**). In addition, features such as mean firing rate (**Figure 5A**) and interspike interval (**Figure 5B**) can be extracted at a single neuron level. Due to the refractory period of neurons (~2 ms) [44], interspike intervals below this threshold were discarded and shown in grey. It is worth emphasizing that given the low number of VANs available for recording, individual neuronal analysis (in contrast to neuronal population descriptive statistics) become more meaningful, particularly due to the diversity in VANs' electrophysiological characteristics. To that end, on a neuronal basis, there is a large variation in mean firing rate (lowest: 0 Hz, max: 23.37 Hz, mean: 1.67 Hz, median: 0.165 Hz) which can possibly be explained due to the various subpopulations of VANs in addition to the range of effector molecules screened here. For this reason, it is important to evaluate the activity at a single neuron level (e.g., via raster plot, heat map) to more accurately reveal the VAN responses. Nevertheless, the heatmap plots of mean firing rate and interspike interval shown in **Figure 5** can be condensed to "population-level" illustration of the VAN activity to reveal general trends of VAN response to effector molecules (**Figure S7**). For example, **Figure S7A** illustrates an increasing trend in mean firing rate from baseline to 5-HT, with a drop at Cap (i.e., desensitization described earlier). This population-level response to Cap is reasonable since a large subpopulation of VANs express the TRPV1 receptor for Cap [24]. **Figure S7B** shows similar characteristics for interspike interval across most of the effector molecules, with a drop at Cap, again highlighting the TRPV1+ subpopulation of VANs.

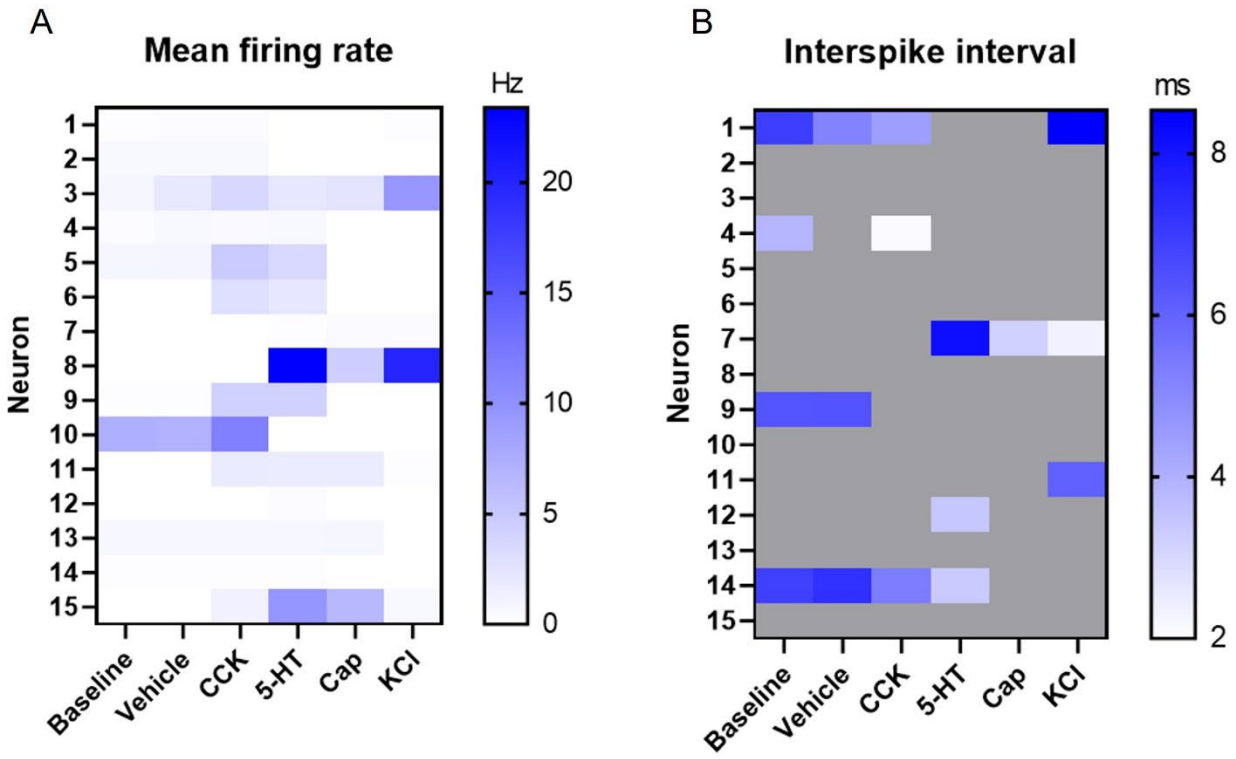

Figure 5. **Extracellular recordings firing characteristics.** (A) Mean firing rate (Hz) for each neuron under each effector molecule group. (B) Interspike interval (ms) for each neuron under each effector molecule group. Interspike intervals below physiological refractory period (2 ms) were discarded and are shown in grey.

4. Conclusions

In this study we demonstrated the ability to harvest primary rat vagal afferent neurons and culture them. We showed that neurons cultured on Matrigel-treated surfaces lead to significant increases in coverage of neuronal processes (e.g., neurites) compared to more classical surface treatment approaches (e.g., PLL coatings). The culture media (serum-based vs. growth factor-based) did not have a significant role in neurite growth or the proliferation of non-neuronal (glial) cells present in the culture. Calcium imaging revealed that the cultured neurons responded to effector molecules suggesting neuronal functionality. We then demonstrated the ability to record extracellular spikes from the VANs under sequential exposure to classical effector molecules as early as DIV1 (unlike 2+ weeks required for cortical cells to exhibit sufficient electrophysiological activity), which is a significant advantage for accelerating experimental timelines. Utilizing both in-house fabricated MEAs and a HD-MEA system, we were able to detect spikes and extract electrophysiological features such as mean firing rate and interspike interval. Collectively, the calcium imaging and electrophysiological recordings revealed the diversity in VANs' responses to effector molecules. We envision that these electrophysiological features can be analyzed with emerging machine learning approaches to eventually attribute distinct electrophysiological fingerprints to individual and mixed effector molecules to serve as cell-based sensors to screen for complex gut-derived effector molecules and therapeutics. As shown here, variations in electrophysiological fingerprints (e.g., Cap desensitization) have physiological connections to the larger *in vivo* system. VANS that are responsive to Cap have been shown to also be sensitive to pathogenic bacterial metabolites [24]. The system described in this study highlights the presence of this population, while also highlighting the presence of other VANs with different electrophysiological signatures. Gut microbiome composition vary across species [45]. However, many bacterial

metabolites/molecules (e.g., short-chain fatty acids, lipopolysaccharide (LPS), neurotransmitters) that create the microbiome remain similar across species. This suggests that while VANs from rats versus human may differ in their responses to these molecules, upon calibration of rat VANs' responses to the effector molecules, they can be broadly used as sensors for microbial metabolites from various species. The response of the VANs can be further specialized to individual species by incorporating other cell types (e.g., human gut immune cells) that occupy the basolateral space adjacent to the VAN nerve terminals. The signals from such supporting cells, which also respond to bacterial metabolites/molecules (e.g., LPS), can further alter the VAN response, therefore providing additional sophistication and species-specificity to the sensing platform. Taken together, we hope that the cell-based electrophysiological sensing approach described here benefit a broad spectrum of gastrointestinal research.

Supplementary Materials: Figure S1: Schematic description of microelectrode array (MEA) fabrication steps. Figure S2: Representative brightfield images of VANs on day *in vitro* 1 grown on the various slide coatings under the various medias; Figure S3: Representative brightfield images of VANs on day *in vitro* 3 grown on the various slide coatings under the various culture media; Figure S4: Immunostained image of day *in vitro* 7 VAN culture, highlighting the presence of a non-neuronal supporting cell (GFAP+); Figure S5: Raster plot for a HD-MEA with no cells (negative control) with a spike frequency cutoff of 6 spikes/min; Figure S6: Intracellular calcium change in fluorescence (ΔF/F %) of KCl after the neurons have already been exposed to Cap; Figure S7: Mean firing rate (Hz) and interspike interval (ms) averaged withing each effector molecule group from the HD-MEA.

Author Contributions: Conceptualization, G.G., D.Z., N.G., H.R. and E.S.; Formal Analysis, G.G. and E.S.; Funding Acquisition, H.R. and E.S.; Investigation, G.G.; Resources, G.G. and N.G.; Software, G.G.; Supervision, H.R. and E.S.; Validation, G.G., D.Z., N.G., H.R. and E.S.; Visualization, G.G.; Writing – Original Draft, G.G.; Writing – Review & Editing, G.G., D.Z., N.G., H.R. and E.S.

Funding: We gratefully acknowledge the support from the National Institutes of Health via NINDS/NIA R03-NS118156 and NCCIH R21-AT010933, and from the National Science Foundation via DMR-2003849.

Institutional Review Board Statement: All procedures involving animals were conducted in accordance with the National Institutes of Health Guide for the Care and Use of Laboratory Animals following the protocol #22421 approved on 4 August 2022 by the University of California, Davis Institutional Animal Care and Use Committee.

Informed Consent Statement: Not applicable.

Data Availability Statement: The datasets generated during and/or analyzed during the current study are available from the corresponding author on reasonable request.

Acknowledgments: We thank Professor James Peters and Rachel Arnold for their technical guidance on harvesting primary VANs. We thank Professor Roy Ben-Shalom and Timothy Fenton for training us to use their HD-MEA system. This project also benefited from the resources of the Center for Nano/Micro-Manufacturing facility at University of California, Davis.

Conflicts of Interest: The authors declare no conflict of interest.

References

1. Cryan, J.F.; Dinan, T.G. Mind-Altering Microorganisms: The Impact of the Gut Microbiota on Brain and Behaviour. *Nat Rev Neurosci* **2012**, *13*, 701–712, doi:10.1038/nrn3346.
2. Goswami, C.; Iwasaki, Y.; Yada, T. Short-Chain Fatty Acids Suppress Food Intake by Activating Vagal Afferent Neurons. *J Nutr Biochem* **2018**, *57*, 130–135, doi:10.1016/j.jnutbio.2018.03.009.
3. Li, Z.; Yi, C.-X.; Katiraei, S.; Kooijman, S.; Zhou, E.; Chung, C.K.; Gao, Y.; van den Heuvel, J.K.; Meijer, O.C.; Berbée, J.F.P.; et al. Butyrate Reduces Appetite and Activates Brown Adipose Tissue via the Gut-Brain Neural Circuit. *Gut* **2018**, *67*, 1269–1279, doi:10.1136/gutjnl-2017-314050.

4. Lee, S.; Knotts, T.A.; Goodson, M.L.; Barboza, M.; Wudeck, E.; England, G.; Raybould, H.E. Metabolic Responses to Butyrate Supplementation in LF- and HF-Fed Mice Are Cohort-Dependent and Associated with Changes in Composition and Function of the Gut Microbiota. *Nutrients* **2020**, *12*, 3524, doi:10.3390/nu12113524.
5. McDougle, M.; Quinn, D.; Diepenbroek, C.; Singh, A.; de la Serre, C.; de Lartigue, G. Intact Vagal Gut-Brain Signalling Prevents Hyperphagia and Excessive Weight Gain in Response to High-Fat High-Sugar Diet. *Acta Physiol (Oxf)* **2021**, *231*, e13530, doi:10.1111/apha.13530.
6. Bonaz, B.; Bazin, T.; Pellissier, S. The Vagus Nerve at the Interface of the Microbiota-Gut-Brain Axis. *Frontiers in Neuroscience* **2018**, *12*.
7. Waise, T.M.Z.; Dranse, H.J.; Lam, T.K.T. The Metabolic Role of Vagal Afferent Innervation. *Nat Rev Gastroenterol Hepatol* **2018**, *15*, 625–636, doi:10.1038/s41575-018-0062-1.
8. Agus, A.; Clément, K.; Sokol, H. Gut Microbiota-Derived Metabolites as Central Regulators in Metabolic Disorders. *Gut* **2021**, *70*, 1174–1182, doi:10.1136/gutjnl-2020-323071.
9. Koh, A.; Vadder, F.D.; Kovatcheva-Datchary, P.; Bäckhed, F. From Dietary Fiber to Host Physiology: Short-Chain Fatty Acids as Key Bacterial Metabolites. *Cell* **2016**, *165*, 1332–1345, doi:10.1016/j.cell.2016.05.041.
10. Buchanan, K.L.; Rupprecht, L.E.; Kaelberer, M.M.; Sahasrabudhe, A.; Klein, M.E.; Villalobos, J.A.; Liu, W.W.; Yang, A.; Gelman, J.; Park, S.; et al. The Preference for Sugar over Sweetener Depends on a Gut Sensor Cell. *Nat Neurosci* **2022**, *25*, 191–200, doi:10.1038/s41593-021-00982-7.
11. Puzan, M.; Hosic, S.; Ghio, C.; Koppes, A. Enteric Nervous System Regulation of Intestinal Stem Cell Differentiation and Epithelial Monolayer Function. *Sci Rep* **2018**, *8*, 6313, doi:10.1038/s41598-018-24768-3.
12. Workman, M.J.; Gleeson, J.P.; Troisi, E.J.; Estrada, H.Q.; Kerns, S.J.; Hinojosa, C.D.; Hamilton, G.A.; Targan, S.R.; Svendsen, C.N.; Barrett, R.J. Enhanced Utilization of Induced Pluripotent Stem Cell-Derived Human Intestinal Organoids Using Microengineered Chips. *Cell Mol Gastroenterol Hepatol* **2018**, *5*, 669-677.e2, doi:10.1016/j.jcmgh.2017.12.008.
13. Newberry, K.; Wang, S.; Hoque, N.; Kiss, L.; Ahlijanian, M.K.; Herrington, J.; Graef, J.D. Development of a Spontaneously Active Dorsal Root Ganglia Assay Using Multiwell Multielectrode Arrays. *J Neurophysiol* **2016**, *115*, 3217–3228, doi:10.1152/jn.01122.2015.
14. Bautista, D.M.; Sigal, Y.M.; Milstein, A.D.; Garrison, J.L.; Zorn, J.A.; Tsuruda, P.R.; Nicoll, R.A.; Julius, D. Pungent Agents from Szechuan Peppers Excite Sensory Neurons by Inhibiting Two-Pore Potassium Channels. *Nat Neurosci* **2008**, *11*, 772–779, doi:10.1038/nn.2143.
15. Ragozzino, F.J.; Arnold, R.A.; Fenwick, A.J.; Riley, T.P.; Lindberg, J.E.M.; Peterson, B.; Peters, J.H. TRPM3 Expression and Control of Glutamate Release from Primary Vagal Afferent Neurons. *Journal of Neurophysiology* **2021**, *125*, 199–210, doi:10.1152/jn.00229.2020.
16. Goshi, N.; Girardi, G.; Souza, F. da C.; Gardner, A.; Lein, P.J.; Seker, E. Influence of Microchannel Geometry on Device Performance and Electrophysiological Recording Fidelity during Long-Term Studies of Connected Neural Populations. *Lab Chip* **2022**, *22*, 3961–3975, doi:10.1039/D2LC00683A.
17. Raybould, H.E.; Zumpano, D.L. Microbial Metabolites and the Vagal Afferent Pathway in the Control of Food Intake. *Physiology & Behavior* **2021**, *240*, 113555, doi:10.1016/j.physbeh.2021.113555.
18. Li, Y. Sensory Signal Transduction in the Vagal Primary Afferent Neurons. *Current Medicinal Chemistry 14*, 2554–2563.
19. Egerod, K.L.; Petersen, N.; Timshel, P.N.; Rekling, J.C.; Wang, Y.; Liu, Q.; Schwartz, T.W.; Gautron, L. Profiling of G Protein-Coupled Receptors in Vagal Afferents Reveals Novel Gut-to-Brain Sensing Mechanisms. *Mol Metab* **2018**, *12*, 62–75, doi:10.1016/j.molmet.2018.03.016.

20. Bai, L.; Mesgarzadeh, S.; Ramesh, K.S.; Huey, E.L.; Liu, Y.; Gray, L.A.; Aitken, T.J.; Chen, Y.; Beutler, L.R.; Ahn, J.S.; et al. Genetic Identification of Vagal Sensory Neurons That Control Feeding. *Cell* **2019**, *179*, 1129-1143.e23, doi:10.1016/j.cell.2019.10.031.
21. Guerville, M.; Hamilton, M.K.; Ronveaux, C.; Ellero-Simatos, S.; Raybould, H.; Boudry, G. Chronic Refined Low-Fat Diet Consumption Reduces Cholecystokinin Satiation in Rats. *European Journal of Nutrition* **2019**, *58*, doi:10.1007/s00394-018-1802-2.
22. Kowalski, C.W.; Lindberg, J.E.M.; Fowler, D.K.; Simasko, S.M.; Peters, J.H. Contributing Mechanisms Underlying Desensitization of Cholecystokinin-Induced Activation of Primary Nodose Ganglia Neurons. *American Journal of Physiology-Cell Physiology* **2020**, *318*, C787–C796, doi:10.1152/ajpcell.00192.2019.
23. Troy, A.E.; Simmonds, S.S.; Stocker, S.D.; Browning, K.N. High Fat Diet Attenuates Glucose-dependent Facilitation of 5-HT3-mediated Responses in Rat Gastric Vagal Afferents. *J Physiol* **2016**, *594*, 99–114, doi:10.1113/JP271558.
24. Riley, T.P.; Neal-McKinney, J.M.; Buelow, D.R.; Konkel, M.E.; Simasko, S.M. Capsaicin-Sensitive Vagal Afferent Neurons Contribute to the Detection of Pathogenic Bacterial Colonization in the Gut. *J Neuroimmunol* **2013**, *257*, 36–45, doi:10.1016/j.jneuroim.2013.01.009.
25. Shreiner, A.B.; Kao, J.Y.; Young, V.B. The Gut Microbiome in Health and in Disease. *Curr Opin Gastroenterol* **2015**, *31*, 69–75, doi:10.1097/MOG.0000000000000139.
26. Simasko, S.M.; Wiens, J.; Karpiel, A.; Covasa, M.; Ritter, R.C. Cholecystokinin Increases Cytosolic Calcium in a Subpopulation of Cultured Vagal Afferent Neurons. *American Journal of Physiology-Regulatory, Integrative and Comparative Physiology* **2002**, *283*, R1303–R1313, doi:10.1152/ajpregu.00050.2002.
27. Ghogha, A.; Bruun, D.A.; Lein, P.J. Inducing Dendritic Growth in Cultured Sympathetic Neurons. *JoVE (Journal of Visualized Experiments)* **2012**, e3546, doi:10.3791/3546.
28. Rienecker, K.D.A.; Poston, R.G.; Saha, R.N. Merits and Limitations of Studying Neuronal Depolarization-Dependent Processes Using Elevated External Potassium. *ASN Neuro* **2020**, *12*, 1759091420974807, doi:10.1177/1759091420974807.
29. Schneider, C.A.; Rasband, W.S.; Eliceiri, K.W. NIH Image to ImageJ: 25 Years of Image Analysis. *Nat Methods* **2012**, *9*, 671–675, doi:10.1038/nmeth.2089.
30. Müller, J.; Ballini, M.; Livi, P.; Chen, Y.; Radivojevic, M.; Shadmani, A.; Viswam, V.; L. Jones, I.; Fiscella, M.; Diggelmann, R.; et al. High-Resolution CMOS MEA Platform to Study Neurons at Subcellular, Cellular, and Network Levels. *Lab on a Chip* **2015**, *15*, 2767–2780, doi:10.1039/C5LC00133A.
31. Pradhananga, S.; Tashtush, A.A.; Allen-Vercoe, E.; Petrof, E.O.; Lomax, A.E. Protease-Dependent Excitation of Nodose Ganglion Neurons by Commensal Gut Bacteria. *J Physiol* **2020**, *598*, 2137–2151, doi:10.1113/JP279075.
32. Daly, D.M.; Park, S.J.; Valinsky, W.C.; Beyak, M.J. Impaired Intestinal Afferent Nerve Satiety Signalling and Vagal Afferent Excitability in Diet Induced Obesity in the Mouse. *J Physiol* **2011**, *589*, 2857–2870, doi:10.1113/jphysiol.2010.204594.
33. Low-Density Neuronal Networks Cultured Using Patterned Poly-l-Lysine on Microelectrode Arrays | Elsevier Enhanced Reader Available online: https://reader.elsevier.com/reader/sd/pii/S0165027006004602?token=2529E54E199303458ACAB8A1EFD344FB7A28719F92ACB7A9ADB3E0F02A0AA2C763F26D56144E1EB501FC8D2AE3E9B5FC&originRegion=us-east-1&originCreation=20230414065150 (accessed on 14 April 2023).

34. Goshi, N.; Morgan, R.K.; Lein, P.J.; Seker, E. A Primary Neural Cell Culture Model to Study Neuron, Astrocyte, and Microglia Interactions in Neuroinflammation. *Journal of Neuroinflammation* **2020**, *17*, 155, doi:10.1186/s12974-020-01819-z.
35. Karahuseyinoglu, S.; Sekerdag, E.; Aria, M.M.; Cetin Tas, Y.; Nizamoglu, S.; Solaroglu, I.; Gürsoy-Özdemir, Y. Three-Dimensional Neuron–Astrocyte Construction on Matrigel Enhances Establishment of Functional Voltage-Gated Sodium Channels. *Journal of Neurochemistry* **2021**, *156*, 848–866, doi:10.1111/jnc.15185.
36. Cooper, E. Synapse Formation among Developing Sensory Neurones from Rat Nodose Ganglia Grown in Tissue Culture. *J Physiol* **1984**, *351*, 263–274.
37. Yakura, T.; Miki, T.; Warita, K.; Ohta, K.; Suzuki, S.; Liu, J.-Q.; Tamai, M.; Takeuchi, Y. Satellite Glial Cells in the Nodose Ganglion of the Rat Vagus Nerve: Morpho- Logical Alterations of Microglial Cells. *Biomed Res* **2013**, *24*.
38. Blackshaw, L.A.; Brookes, S.J.H.; Grundy, D.; Schemann, M. Sensory Transmission in the Gastrointestinal Tract. *Neurogastroenterology & Motility* **2007**, *19*, 1–19, doi:10.1111/j.1365-2982.2006.00871.x.
39. Wei, Z.; Lin, B.-J.; Chen, T.-W.; Daie, K.; Svoboda, K.; Druckmann, S. A Comparison of Neuronal Population Dynamics Measured with Calcium Imaging and Electrophysiology. *PLoS Comput Biol* **2020**, *16*, e1008198, doi:10.1371/journal.pcbi.1008198.
40. Heinricher, M.M. Principles of Extracellular Single-Unit Recording.
41. Atmaramani, R.; Chakraborty, B.; Rihani, R.T.; Usoro, J.; Hammack, A.; Abbott, J.; Nnoromele, P.; Black, B.J.; Pancrazio, J.J.; Cogan, S.F. Ruthenium Oxide Based Microelectrode Arrays for in Vitro and in Vivo Neural Recording and Stimulation. *Acta Biomaterialia* **2020**, *101*, 565–574, doi:10.1016/j.actbio.2019.10.040.
42. Obien, M.E.J.; Deligkaris, K.; Bullmann, T.; Bakkum, D.J.; Frey, U. Revealing Neuronal Function through Microelectrode Array Recordings. *Frontiers in Neuroscience* **2015**, *8*.
43. Sasamura, T.; Kuraishi, Y. Peripheral and Central Actions of Capsaicin and VR1 Receptor. *The Japanese Journal of Pharmacology* **1999**, *80*, 275–280, doi:10.1254/jjp.80.275.
44. Hampel, D.; Lansky, P. On the Estimation of Refractory Period. *Journal of Neuroscience Methods* **2008**, *171*, 288–295, doi:10.1016/j.jneumeth.2008.03.003.
45. Nagpal, R.; Wang, S.; Solberg Woods, L.C.; Seshie, O.; Chung, S.T.; Shively, C.A.; Register, T.C.; Craft, S.; McClain, D.A.; Yadav, H. Comparative Microbiome Signatures and Short-Chain Fatty Acids in Mouse, Rat, Non-Human Primate, and Human Feces. *Front Microbiol* **2018**, *9*, 2897, doi:10.3389/fmicb.2018.02897.

biosensors

MDPI

Supporting Information

Cultured Vagal Afferent Neurons as Sensors for Intestinal Effector Molecules

Gregory Girardi, Danielle Zumpano, Noah Goshi, Helen Raybould and Erkin Seker *

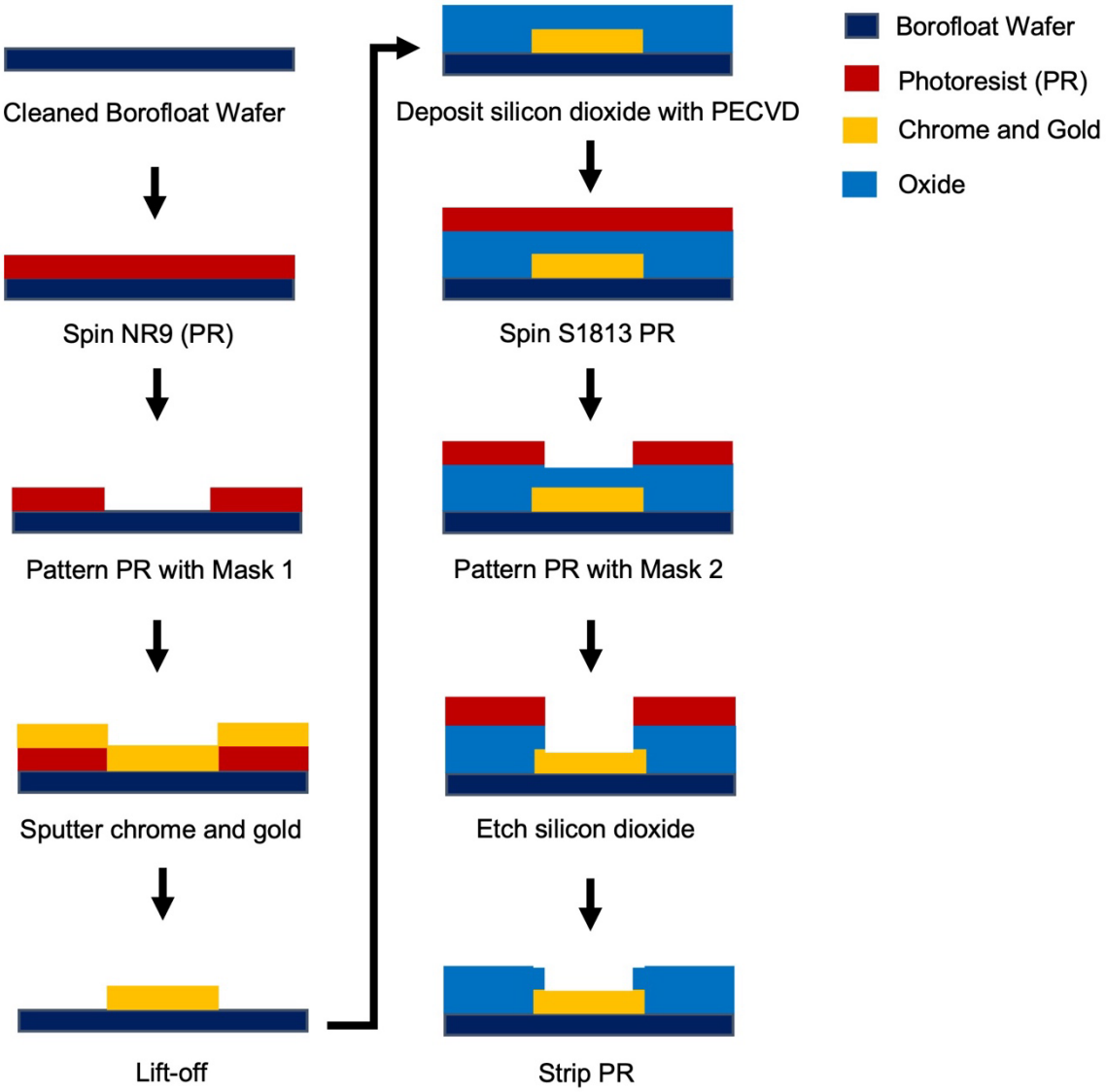

Figure S1. **Schematic of microelectrode array fabrication steps.** Cleanroom techniques including thin-film metal deposition and photolithography were used to fabricate custom microelectrode arrays. Briefly, gold with a chrome adhesion layer was deposited onto a glass wafer to pattern the electrodes (mask 1), silicon oxide was deposited to insulate the electrodes, and opened only above the recording regions (mask 2) with a buffered oxide etch (BOE).

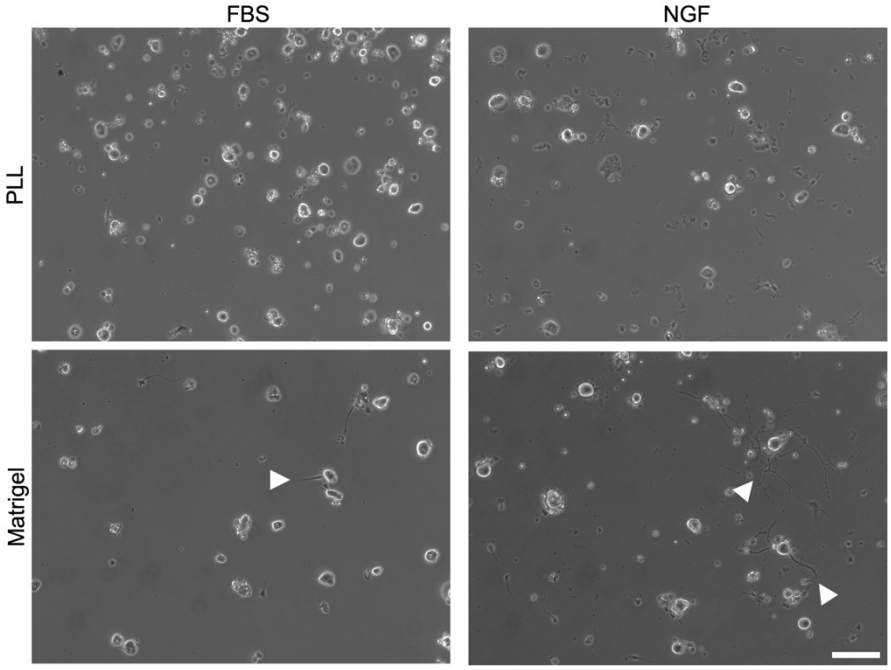

Figure S2. **Day 1 VAN culture.** Media comparison of serum-based media (DMEM +FBS) to growth factor-based (DMEM/F12 +NGF). White triangles indicate neurite outgrowth. Scale bar 100 μm.

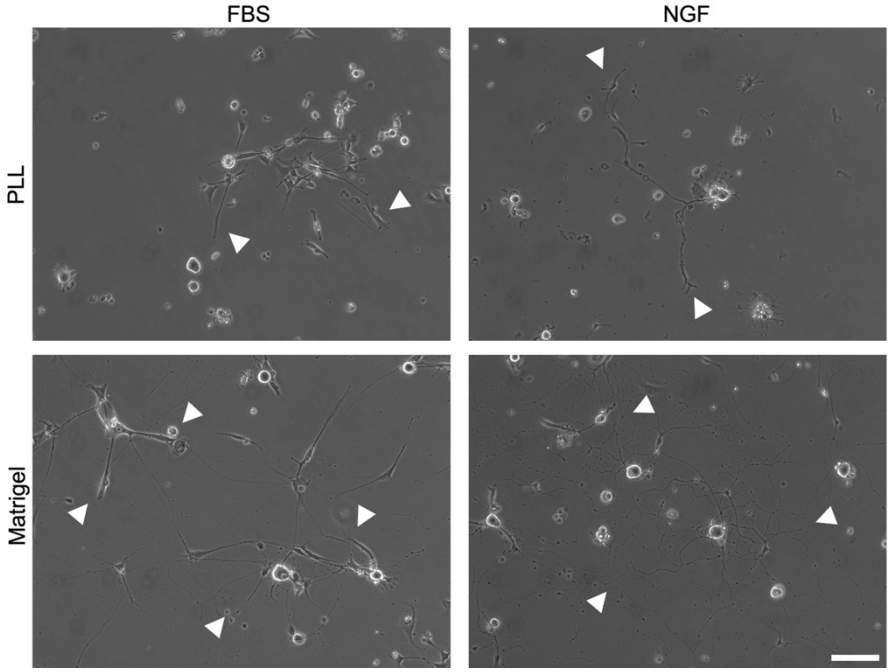

Figure S3. **Day 3 VAN culture.** Media comparison of serum-based media (DMEM +FBS) to growth factor-based (DMEM/F12 +NGF). White triangles indicate neurite outgrowth. Scale bar 100 μm.

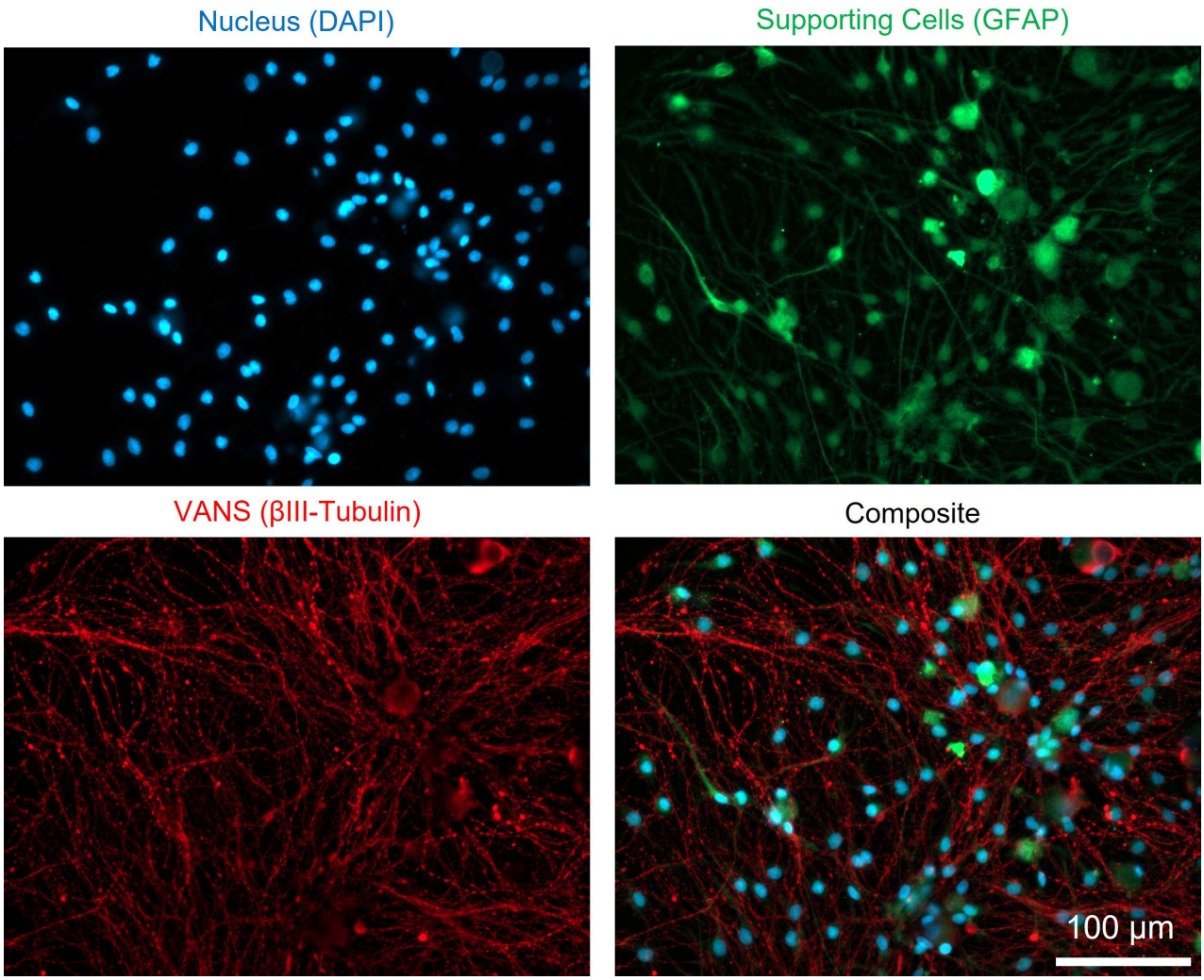

Figure S4. **Day 7 VAN culture.** Immunostained (DAPI – nuclei, GFAP – supporting cell, βT-III – neuron) VAN culture on day in vitro 7 highlighting that at longer culture durations, non-neuronal supporting and proliferative cells (GFAP+) are present. Scale bar 100 µm.

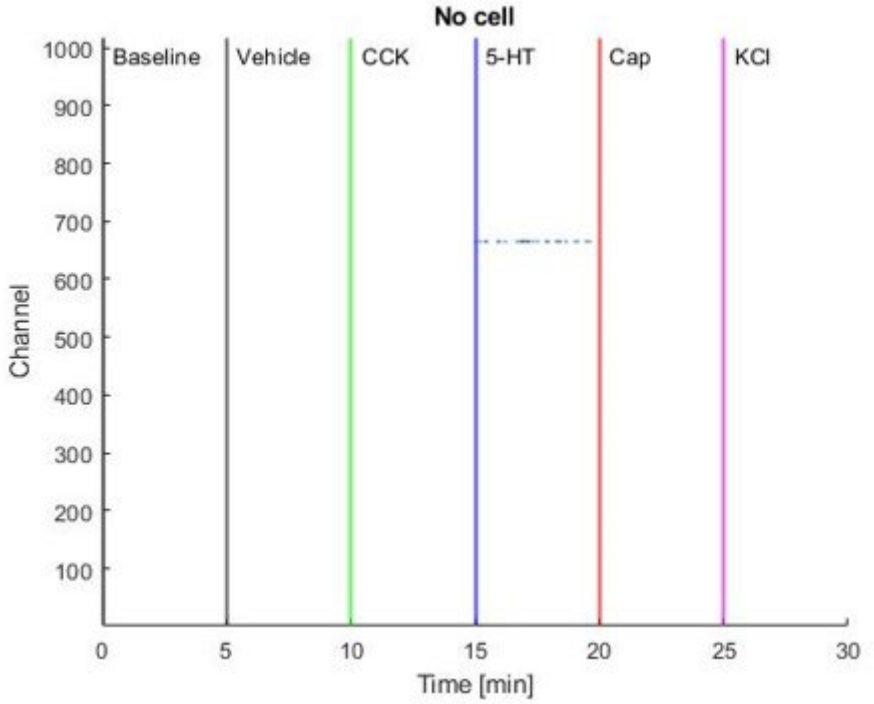

Figure S5. **Raster plot for HD-MEA chip with no cells.** A chip containing no cells shows negligible signal. Allowing us to trust that our signals recorded from chips with cells are real cellular signals.

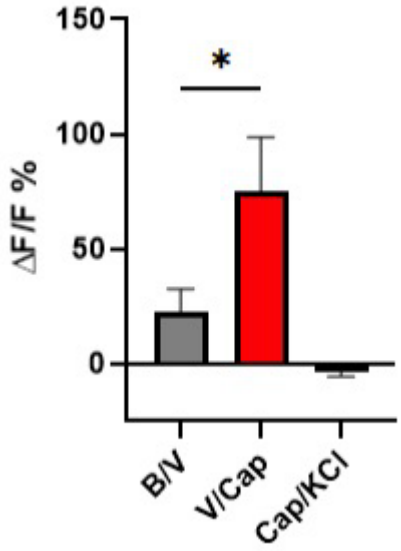

Figure S6. **Intracellular calcium response after Cap exposure.** Elevated extracellular potassium (20 mM) after Cap (1 μM) exposure does not change ΔF/F %. Highlighting that these neurons became desensitized from Cap. * $P \leq 0.05$.

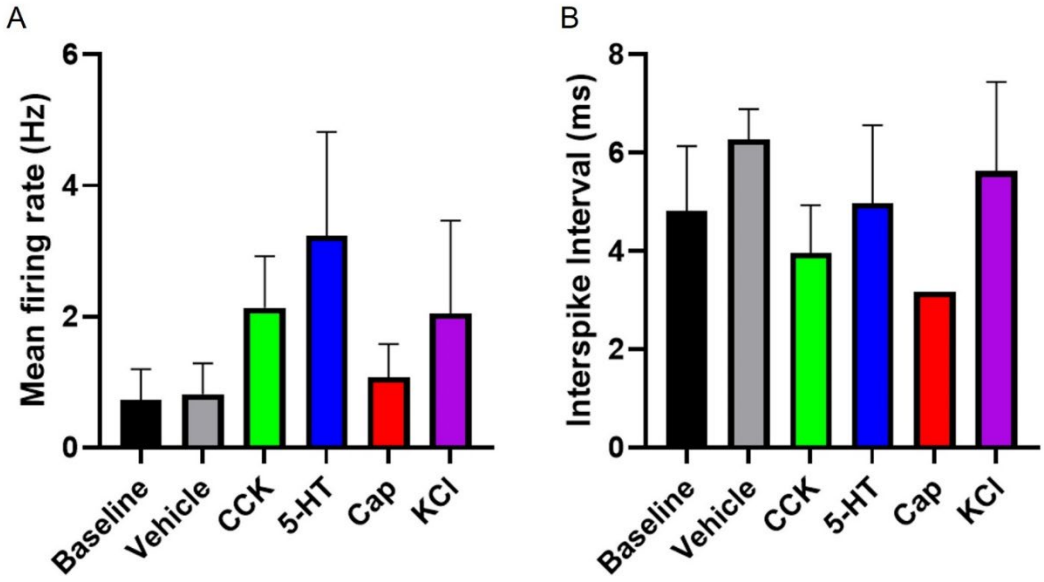

Figure S7. **Averaged extracellular recordings firing characteristics.** (A) Mean firing rate (Hz) under each effector molecule group, highlighting the increase in firing rate from CCK, 5-HT, and KCl, while also showcasing the drop-in mean firing rate under Cap. (B) Interspike interval (ms) under each effector molecule group showcasing the decrease in interspike interval under Cap.